Construction and Building Materials 201 (2019) 631–640

Contents lists available at ScienceDirect

Construction and Building Materials

journal homepage: www.elsevier.com/locate/conbuildmat

Tailoring engineered cementitious composite with emulsified asphalt for high damping

Hui Ma [a,b], Shunzhi Qian [c,*], Victor C. Li [d]

[a] Jiangsu Expressway Engineering Maintenance Technology Co. Ltd, Nanjing 211106, PR China
[b] School of Materials Science and Engineering, Southeast University, Nanjing 210096, PR China
[c] School of Civil and Environmental Engineering, Nanyang Technological University, Singapore 639798, Singapore
[d] Department of Civil and Environmental Engineering, University of Michigan, 2132 G.G. Brown Building, Ann Arbor, MI 48109, USA

HIGHLIGHTS

- Incorporating EA in ECC effectively increases loss modulus and loss factor.
- EA-ECC has superior tensile ductility and similar loss factor when compared with CA with similar EA dosage.
- Tensile ductility of EA-ECCs improve significantly with increase dosage of EA.
- Temperature has similar effect on strength and ductility as compared to EA.
- EA-ECC can potentially be used as vibration absorbing layer in high speed railway.

ARTICLE INFO

Article history:
Received 24 October 2018
Received in revised form 28 December 2018
Accepted 31 December 2018

Keywords:
Engineered cementitious composite (ECC)
Emulsified asphalt (EA)
Strain-hardening behavior
Dynamic mechanical thermo-analysis
Temperature

ABSTRACT

Cement asphalt (CA) mortar has been widely used as cushion layer between the concrete roadbed and track slab for vibration absorption in high-speed railways (HSR). However, premature cracking of CA has been recognized as a critical safety problem during HSR operation. There is a need for developing more durable materials with similar damping ability and vibration absorption characteristics as CA mortar. This paper reports the development of emulsified asphalt (EA) modified Engineered cementitious composite (EA-ECC) with favorable damping property, which may be used as vibration absorbing layer material. The mechanical properties, including compressive strength, tensile stress-strain relation and dynamic mechanical properties of EA-ECCs were investigated. It is found that the desirable higher loss modulus and loss factor are accompanied by lower compressive and tensile strength with increase of EA dosage. Conversely, the deformation capacity of EA-ECCs shows an opposite trend due to favorable change in interfacial properties. In addition, with increasing test temperature, the material also shows a trend similar to the addition of EA. Change of microstructures of EA-ECCs were also observed through scanning electron microscope (SEM) imaging. It is concluded that incorporating EA significantly improves the tensile ductility and energy dissipation ability of ECC materials. Increase of 210 times in tensile ductility and similar loss factor are demonstrated when compared with those of CA with similar EA dosage.
© 2019 Elsevier Ltd. All rights reserved.

1. Introduction

Engineered cementitious composite (ECC) is a special kind of high performance fiber reinforced cementitious composite (HPFRCC), which was developed by Li and co-workers in the 1990s [1]. ECC is designed based on micromechanics and fracture mechanics [2,3]. It can reach a compressive strength of 40–210 MPa depending on the mixture proportion [4,5]. In addition, ECC has extreme tensile ductility, in the range of 3–8% (300–800 times that of concrete or FRC) [6]. After first cracking, the crack width stabilizes at about 30–100 μm while the number of cracks increases, which is the source of the excellent tensile strain capacity of ECC material [7]. Unlike normal concrete and fiber reinforced concrete, tight crack width is an intrinsic material property of ECC, independent of structure size, steel reinforcement, or ambient load. ECC has been applied in the repair of concrete structures (dam and bridge pier etc.), and in applications such as

* Corresponding author at: School of Civil and Environmental Engineering, Nanyang Technological University, Singapore 639798, Singapore.
E-mail addresses: zephyor@gmail.com, szqian@ntu.edu.sg (S. Qian).

https://doi.org/10.1016/j.conbuildmat.2018.12.222
0950-0618/© 2019 Elsevier Ltd. All rights reserved.

coupling beams in high rise building [8], and as link slabs on bridge decks [9].

Cement asphalt (CA) mortar, a kind of cementitious mortar modified by emulsified asphalt (EA) and chemical admixtures, is widely used as a cushion layer of non-ballast slab track on high-speed railways in many countries such as Japan, Germany and China [10,11]. CA mortar has a high loss modulus and serves as the energy dissipation layer injected between the roadbed and track slab, which significantly impacts the safety, stability and ride comfort of the non-ballast slab track [10,12]. However, during the service life of track slab, vehicle dynamic load, mismatch of thermal expansion and temperature gradient often lead to premature damages/cracks or deterioration in the CA mortar layer. In Chinese high speed railway lines, for instance, damages of CA mortar layer have been recognized as one of the most critical problems after a period of operation [13]. These damages not only increase maintenance cost, but also potentially impact the safe operation of high speed railways.

To address these issues in CA mortar, it was proposed to develop a new cementitious composite material combining the advantages of CA mortar and ECC material, i.e. EA modified ECC (EA-ECC). In other words, the developed new composite material should be able to offer the desired high damping property while maintaining high tensile strain and tight crack under dynamic loads, which will increase the fracture resistance and durability of non-ballast slab track. Specifically, the influence of EA on the mechanical properties of EA-ECCs, including compressive strength, tensile stress-strain relation, and dynamic mechanical properties, were investigated. The microstructures and interfacial properties between PVA fiber and matrix of EA-ECCs were observed via scanning electron microscope (SEM) imaging and single fiber pullout test, respectively. In addition, as EA is a temperature sensitive material, the influence of test temperature on EA-ECC's mechanical properties was also investigated in this study.

2. Experimental programs

2.1. Raw materials

Type I Ordinary Portland Cement and type I fly ash according to Chinese standards [14,15] were used in this study, and their chemical compositions provided by manufacturer are listed in Table 1. The fine silica sand with the size distribution of 106–212 μm and a mean size of 150 μm was used. A styrene-butadienestyrene (SBS) modified EA was added in EA-ECCs. The technical properties of EA are listed in Table 2, which meet the Chinese standard requirement [16]. In order to control the workability of fresh EA-ECC mixtures, the polycarboxylate-based high range water reducing admixture (HRWRA) was used. PVA fiber (with a surface coating of 1.2% by weight) was used in this study, and its physical and mechanical properties are listed in Table 3.

2.2. Mix proportion and specimen preparation

The mix proportions of EA-ECCs investigated in this study are given in Table 4. The EA-ECC mixtures were modified based on the ECC version in the work of Li and coworkers [5,17]. The ratio of fly ash to cement (FA/C) was fixed at 1.2. The volume fraction of PVA fiber was 2% by total EA-ECC mixture. EA was added at five different dosages (by weight of cement), and the corresponding volume of EA in terms of total volume is 0%, 2.9%, 5.6%, 8.3% and 13.6%, respectively. In order to keep the same ratio of water to cementitious materials (cement and fly ash in this study), the water content was adjusted according to the dosage of EA which has a moisture content of 36.8% (solid content of 63.8% according to Table 2).

Table 2
Technical properties of SBS modified emulsified asphalt.

Property		Value
Density (g/cm^3)		1.02
Sieve residue of 1.18 mm (%)		0.03
Standard viscosity C25.3 (s)		14
Storage stability 1d (%)		0.02
Evaporative residue	Solid content (%)	63.2
	Penetration at 25 °C(0.1 mm)	74
	Soft point (°C)	49.2
	Ductility at 15 °C (cm)	66

All EA-ECC mixtures were prepared using a planetary mixer of 10 L capacity. All solid ingredients, including cement, silica sand and fly ash, were first mixed for 3 min. The mixture of water and EA were then added and mixed for 5 min. At the same time, the high range water reducing admixture was added to adjust the workability. When the fresh mortar reached a homogeneous state, the PVA fibers were added slowly and mixed for 10 more minutes until the fibers were evenly distributed. All specimens were demolded after 24 h, and then cured under sealed condition at 95 ± 5% RH and 20 ± 2 °C until the predetermined testing age of 28 days.

2.3. Test methods

The compressive and uniaxial tensile tests were conducted to investigate the influence of EA dosage on EA-ECCs' mechanical properties. The cube specimen with the size of 70.7 × 70.7 × 70.7 mm^3 was prepared for compressive test. Three samples were tested for each mix. The test was conducted using a hydraulic testing machine with a load capacity of 2000 kN.

To investigate the tensile stress-strain relation of EA-ECCs, the uniaxial tensile test was conducted using a 20 kN SANS test machine. The tensile test setup and specimen dimension are shown in Fig. 1. Two LVDTs were attached on both sides of the specimen to measure the deformation of EA-ECC sample. The test was conducted under displacement control at a rate of 0.5 mm/min as recommended by the Japan Society of Civil Engineers (JSCE) [18]. In order to investigate the effects of EA on EA-ECCs' microstructures, the scanning electron microscopy (SEM) imaging technique was used.

In order to gain a deeper understanding on the influence of EA on EA-ECCs' mechanical properties, interfacial parameters, including chemical bonding G_d and frictional bond strength τ_0, were measured through single fiber pullout test. The produce for the single fiber pullout test follows that of Ma et al. [19], and the calculation procedures of the interfacial parameters followed that of Redon et al. [20]. The matrix (EA-ECC without PVA fiber) parameters, including elastic modulus E_m and fracture strength σ_{fc}, were

Table 1
Chemical compositions of cement and fly ash (by percent).

Material	SiO_2	Al_2O_3	Fe_2O_3	CaO	SO_3	P_2O_5	Na_2O	K_2O	TiO_2	MgO
Cement	21.26	7.67	2.88	57.82	4.04	5.26	0	0.78	0.21	–
Fly ash	52.25	27.42	4.84	7.22	1.83	0.89	0.4	1.32	1.10	2.57

Table 3
Physical and mechanical properties of PVA fiber.

Diameter (μm)	Length (mm)	Elongation (%)	Density (g/cm^3)	Elastic Modulus (GPa)	Tenacity (MPa)
39	12	7	1.3	42.8	1620

Table 4
Mix proportions of EA-ECCs (by weight).

Mix No.	C	FA	Sand	Water	HRWRA	PVA fiber*	EA
EA-ECC0	1	1.2	0.8	0.55	0.02	2%	0
EA-ECC5	1	1.2	0.8	0.52	0.02	2%	0.05
EA-ECC10	1	1.2	0.8	0.49	0.02	2%	0.10
EA-ECC15	1	1.2	0.8	0.46	0.02	2%	0.15
EA-ECC25	1	1.2	0.8	0.40	0.02	2%	0.25

Note: *PVA fibers were added by volume of total EA-ECC mixture.

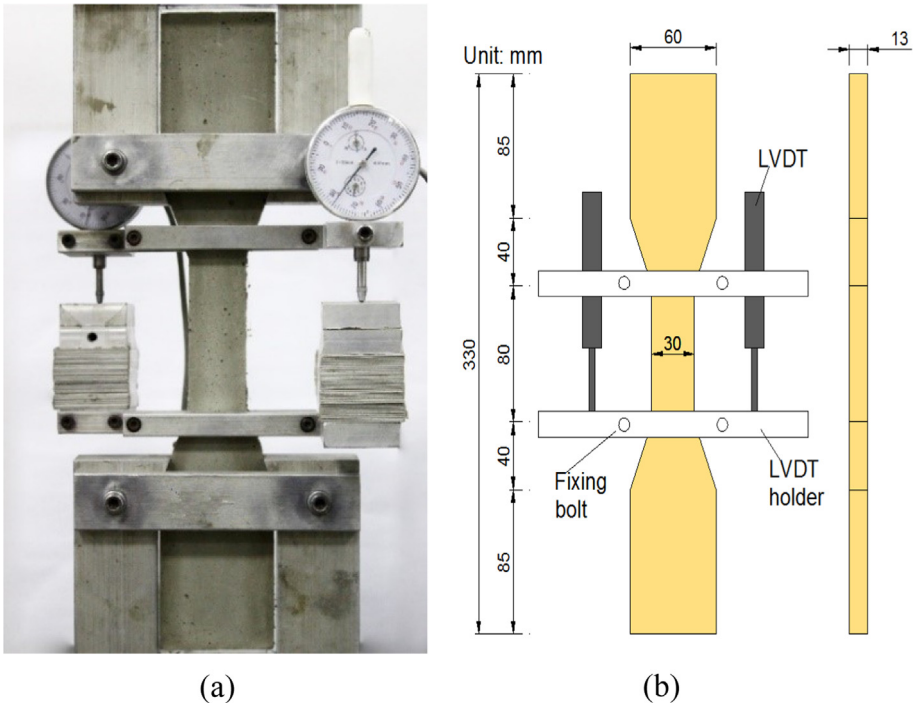

Fig. 1. Uniaxial tensile test on EA-ECC dog-bone specimen: (a) test setup and (b) specimen dimension.

measured by uniaxial tensile test on matrix specimen, which has the same dimensions as EA-ECC dog-bone specimen. Tensile strain capacity of matrix with EA (CA mortar) was also measured through this tensile test. In addition, the fracture toughness K_m of matrix was measured by three point bending test following a procedure similar to that described in ASTM E399 [21].

The dynamic mechanical properties of EA-ECCs, including storage modulus, loss modulus and loss factor (tan δ), were analyzed using dynamic thermo-mechanical analysis instrument (DMA Q800). The specimens were prepared through incising from the coupon specimens, and have a length of 60 ± 3 mm, width of 13 ± 3 mm, and thickness of 2–3 mm. Three specimens were prepared for each EA-ECC mixture. Both ends of the specimen were fixed and under a middle point load during the test. Schematic test setup is shown in Fig. 2. The load is applied in sinusoidal form with an amplitude of 3 μm and frequency of 6 Hz. During the test, chamber temperature increased from −40 °C to 80 °C at speed of 2 °C/min [22].

EA-ECC10 was selected to investigate the influence of test temperature on EA-ECC's mechanical properties (compressive strength

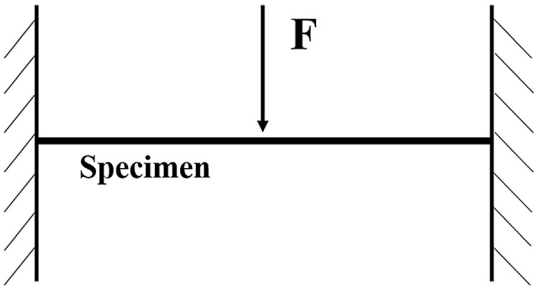

Fig. 2. Schematic test setup of middle point load with both ends fixed.

and tensile stress-strain relation). Firstly, all EA-ECC10 specimens were cured at 95 ± 5% RH and 20 ± 2 °C for 28 days, which ensures that all the cementitious parts have the same degree of hydration. The EA-ECC10 specimens were then conditioned at 0 °C, 25 °C and 60 °C in an environmental chamber of universal test machine (UTM-25) for 2 h before testing. Compressive strength test was

conducted on the specimen immediately after removing from the chamber, using a hydraulic testing machine. The uniaxial tensile test was conducted using the UTM-25 with the specimen in the environmental chamber.

3. Results and discussions

3.1. Compressive strength

The influence of EA dosage on compressive strength of EA-ECCs is shown in Fig. 3, which reveals a slight reduction when the EA/C increases from 0% to 10%, followed by a significant drop when the EA/C increases form 10% to 25%. The compressive strength of EA-ECC25 is 32 MPa, reduced by 45% compared to that of EA-ECC0 (without EA). There are a number of mechanisms to explain the reduction of compressive strength in EA-ECCs. Firstly, the continuous asphalt phase in composite retard the link of cementitious hydration products (C-S-H), therefore C-S-H could not form a strong network (the compressive strength formation mechanism) [12]. Secondly, excessive emulsified asphalt may form a membrane wrapping cementitious particles, which isolates cementitious particles from water, resulting in a lower degree of hydration [23]. Thirdly, as EA/C increases, the fluidity of EA-ECC mortar decreases and more air bubbles will enter the EA-ECC mixture during the process of mixing and molding [24], which will lead to lower compressive strength.

3.2. Tensile stress-strain relation

Table 5 summarizes the uniaxial tensile test results on EA-ECCs. The tensile stress-strain curves of EA-ECCs are shown in Fig. 4. From Table 5, the first cracking strength (the stress corresponding to the first non-linear point/load drop-off of the tensile stress-strain curve) of EA-ECCs is shown to reduce with increasing EA dosage. At 25% EA, the first cracking strength drops to 2.83 MPa, a 27% reduction compared to that of EA-ECC0. The first cracking strength of ECC is mainly governed by the matrix fracture strength. As described in the prior section, incorporating EA likely causes a higher porosity microstructure of matrix and a weak network of C-S-H, which results in lower matrix fracture strength and first cracking strength of EA-ECCs.

As can be seen in Fig. 4, EA-ECCs exhibit improved tensile strain-hardening behavior with increasing EA dosage. While the tensile strength of EA-ECCs has a slight reduction, tensile strain capacity shows a significant increase with increasing EA dosage. From Table 5, tensile strength of EA-ECC reduces slightly from 5.15 MPa (EA-ECC0) to 4.3 MPa (EA-ECC25). Conversely, tensile strain capacity of EA-ECC25 reaches 6.34%, which increases by 3 times compared to that of EA-ECC0. In addition, it is 210 times over the tensile strain capacity of the CA mortar (matrix with 25% EA) of 0.03%.

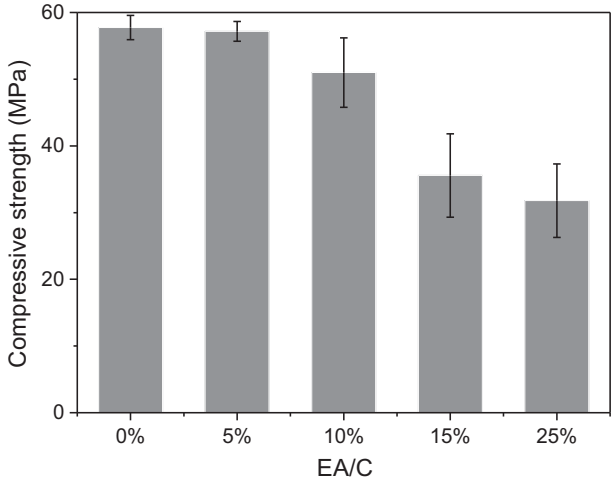

Fig. 3. Compressive strength of EA-ECCs versus EA dosage. A significant drop in compressive strength can be observed when EA exceeded 10% of cement weight.

Table 5
Uniaxial tensile test results of EA-ECCs.

EA-ECC No.	First cracking strength (MPa)	Tensile strength (MPa)	Tensile strain capacity (%)
EA-ECC0	3.86 ± 0.57	5.15 ± 0.37	1.61 ± 0.38
EA-ECC5	3.84 ± 0.52	5.35 ± 0.49	2.61 ± 0.19
EA-ECC10	3.63 ± 0.42	4.50 ± 0.08	3.32 ± 0.98
EA-ECC15	3.50 ± 0.01	4.40 ± 0.40	4.44 ± 1.65
EA-ECC25	2.83 ± 0.32	4.32 ± 0.38	6.34 ± 0.28

Tensile strength of EA-ECC is governed by fiber bridging capacity σ_0 on the weakest crack plane. Furthermore, according to Li and Leung [2], fiber bridging capacity is closely related to interfacial bond between fiber and matrix, assuming no fiber rupture. The reduction of tensile strength may be attributed to weakened fiber/-matrix interfacial bond when EA is added. Fig. 5 shows the interfacial chemical bonding G_d of EA-ECCs, including observed value, average value and coefficient of variation, at different EA dosage. It shows a slight decreasing of interfacial chemical bonding G_d when incorporating EA. The chemical bonding itself is governed by the metal cation concentration, in particular Al^{3+} and Ca^{2+}, in the interface between PVA fiber and cementitious matrix [5]. It was found that Al^{3+} and Ca^{2+} are responsible for the formation of a strong thin layer interface between cement grain and PVA bulk polymer [25,26]. As discussed in the prior section, incorporating EA loosens the matrix microstructure, which may further results in a higher micro-porosity on fiber/matrix interface. The high porosity interface reduces the contact area between PVA fiber and matrix and metal cation concentration on interface, which result in a lower chemical bonding.

Fig. 6 shows the frictional bond strength τ_0 of EA-ECCs, including observed value, average value and coefficient of variation, at different EA dosage. As can be seen, frictional bond strength τ_0 decreases significantly when EA dosage increases from 5% to 10%. Frictional bond strength is closely related to the compactness and roughness of interfacial transition zone (ITZ) between fiber and matrix [27]. For EA-ECCs in this study, an asphalt membrane was formed on ITZ, which reduces the roughness of ITZ. As can be seen in Fig. 7, the fiber/matrix interface in EA-ECC0 is rougher than that in EA-ECC25. Lower roughness of ITZ causes the reduction of frictional bond strength. In addition, Fig. 8 shows the surface conditions of PVA fibers in ECC without and with EA. As can be seen, the PVA fiber surface is damaged significantly after being pulled out due to high frictional bond strength in EA-ECC0, while the PVA fiber surface remains intact in EA-ECC25. It further confirms that incorporating EA reduces the frictional bond strength.

According to the fiber bridging model developed by Yang et al. [28], fiber bridging stress versus crack opening curves of EA-ECCs can be shown in Fig. 9 based on the micromechanical parameters described above. As can be seen in this figure, the peak bridging stress (fiber bridging capacity) shows an obvious reduction when EA is added with a dosage over 10%, which is consistent with tensile strength result of EA-ECCs.

According to the design theory of ECC, to acquire an excellent tensile strain-hardening behavior in EA-ECCs, the strength criterion and energy criterion should be satisfied [2,28]. The strength criterion requires that the first cracking strength controlled by matrix fracture strength σ_{fc} to be less than the fiber bridging capacity σ_0 on the weakest crack plane, as shown in Eq. (1).

$$\sigma_{fc} \leq \sigma_0 \tag{1}$$

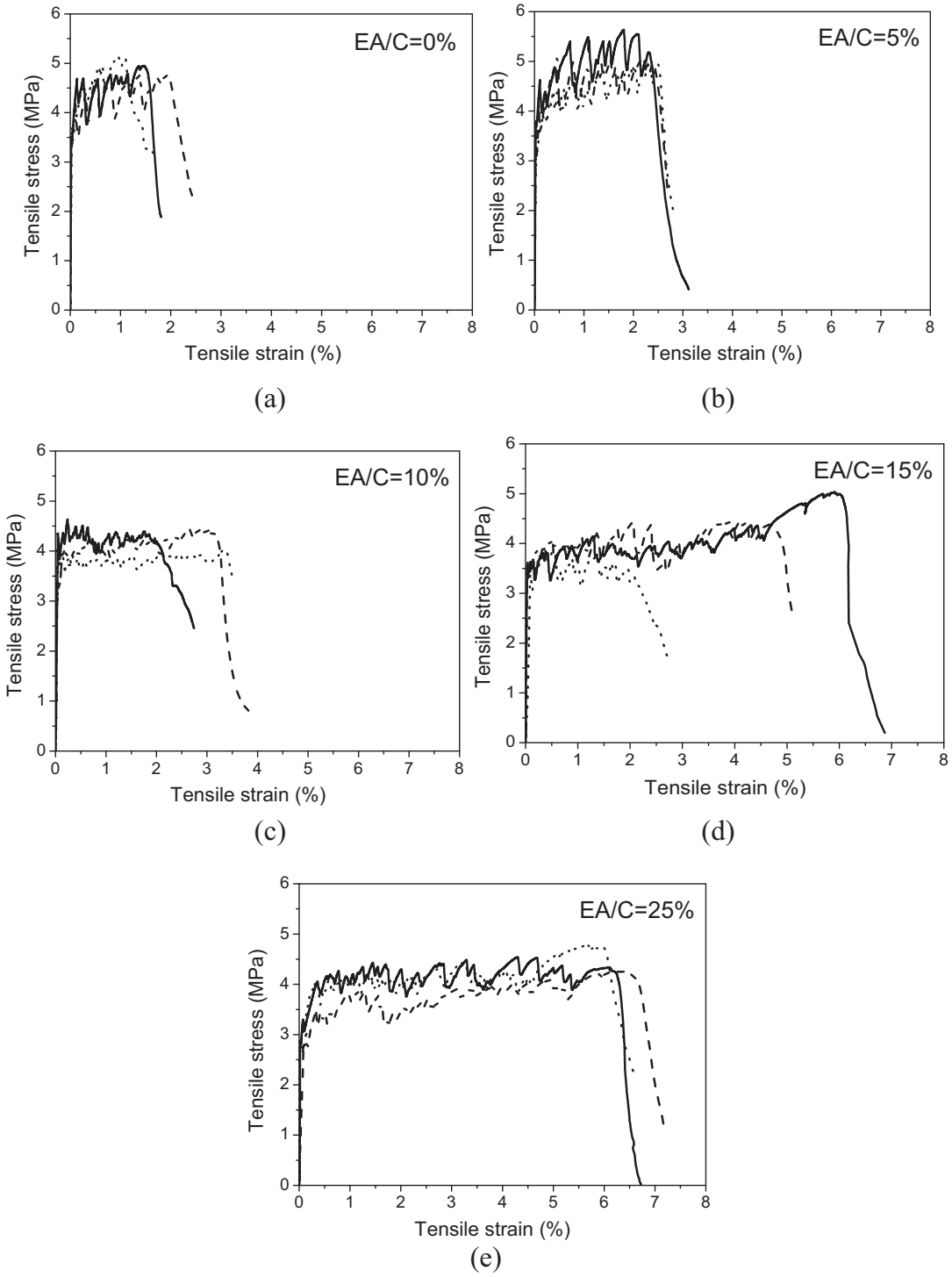

Fig. 4. Typical uniaxial tensile stress-strain curves of EA-ECCs: (a) EA-ECC0; (b) EA-ECC5; (c) EA-ECC10; (d) EA-ECC15; (e) EA-ECC25. With increase in EA/C, first cracking and tensile strength decrease while tensile strain capacity increases.

The energy criterion requires the crack tip toughness J_{tip} to be less than the complementary energy J_b', as shown in Eq. (2). The J_{tip} and J_b' are illustrated in Fig. 10. In the figure σ_{ss} is the steady state cracking stress; δ_{ss} is the flat crack opening corresponding to σ_{ss}; σ_0 is the maximum bridging stress which corresponds to the crack opening δ_0.

$$J_{tip} \leq J_b' \tag{2}$$

In order to quantitatively evaluate tensile strain-hardening behavior of ECC, pseudo strain-hardening performance indexes (PSH) were proposed by Kanda and Li [29], as shown in Eq. (3). Generally speaking, a higher PSH index enhances tensile strain-hardening behavior of ECC.

$$PSH_{energy} = \frac{J_b'}{J_{tip}} \;\&\; PSH_{strength} = \frac{\sigma_0}{\sigma_{fc}} \tag{3}$$

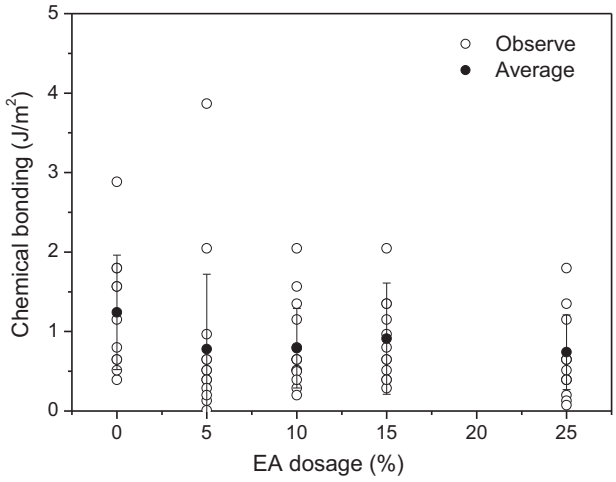

Fig. 5. Chemical bonding G_d of EA-ECCs versus EA dosage.

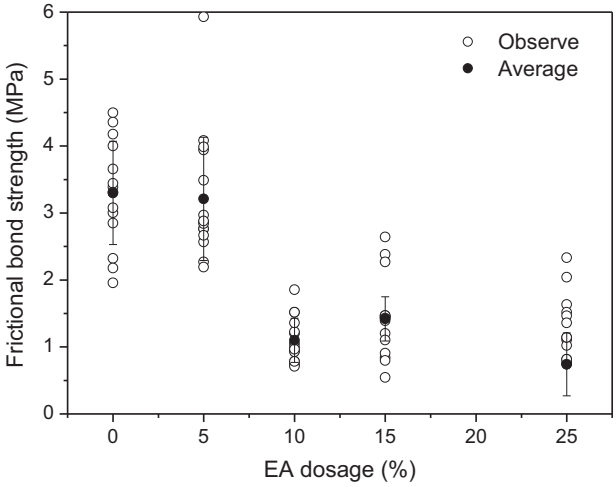

Fig. 6. Frictional bond strength of EA-ECCs versus EA dosage.

Incorporating EA improves tensile strain-hardening behavior, especially for tensile strain capacity, can also be reflected by the increase of PSH indexes. Based on the fiber bridging model mentioned above, the complementary energy J_b' and fiber bridging capacity σ_0 of EA-ECCs can be calculated. The matrix fracture strength σ_{fc} was obtained from uniaxial tensile test on matrix specimen. The crack tip toughness J_{tip} can be approximated as the cementitious matrix toughness if fiber volume fraction is less than 5%, as calculated in Eq. (4) [30].

$$J_{tip} = \frac{K_m^2}{E_m} \tag{4}$$

where K_m is the matrix fracture toughness, which was obtained through three point bending test on notched prism specimen. E_m is the matrix elastic modulus, which was calculated based on the results of uniaxial tensile test on matrix specimen. The PSH indices as a function of EA dosage were obtained, as shown in Fig. 11. As can be seen, both PSH_{energy} and $PSH_{strength}$ reveal pronounced ascending trend with increasing EA dosage. Higher PSH indexes mean the energy criterion and strength criterion can be satisfied with a larger margin, which governs steady-state flat crack propagation and multiple cracking in EA-ECCs. The multiple steady-state cracks are the source of tensile strain capacity. Hence, Fig. 11 explains why EA-ECCs show more excellent tensile strain-hardening behavior with increasing EA dosage.

3.3. Dynamic thermo-mechanical analysis of EA-ECCs

When a viscoelastic material is subjected to a sinusoidal stress, it responds with delayed strain, as shown in Fig. 12. The stress and strain are given by Eq. (5) [31].

$$\begin{cases} \sigma(t) = \sigma_0 \sin(\omega t + \delta) \\ \varepsilon(t) = \varepsilon_0 \sin \omega t \end{cases} \tag{5}$$

where $\sigma(t)$ and $\varepsilon(t)$ is stress and strain with time, respectively; σ_0 and ε_0 is amplitude of sinusoidal stress and strain, respectively; ω is angle velocity, and δ is phase angle.

The complex modulus of viscoelastic material is expressed as:

$$E^* = \frac{\sigma(t)}{\varepsilon(t)} = \frac{\sigma_0}{\varepsilon_0}(\cos\delta + i\sin\delta) = E' + iE'' \tag{6}$$

where E' is the elastic or storage modulus which characterizes the elastic behavior of the material, is proportional to the energy stored by each loading cycle; E'' is the viscous or loss modulus which characterizes the viscous behavior of the material, is proportional to the energy dissipated by each loading cycle. They can be expressed as follows:

$$\begin{cases} E' = \frac{\sigma_0}{\varepsilon_0}\cos\delta \\ E'' = \frac{\sigma_0}{\varepsilon_0}\sin\delta \end{cases} \tag{7}$$

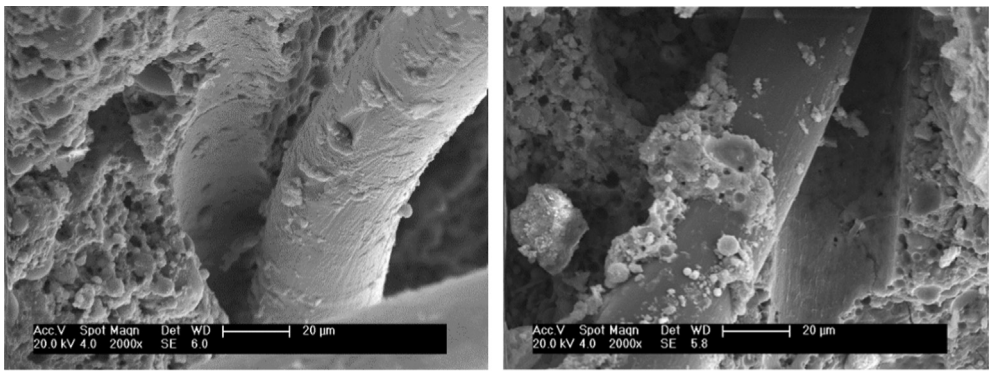

Fig. 7. Fiber/matrix interface in EA-ECCs: (a) EA/C = 0%; (b) EA/C = 25%.

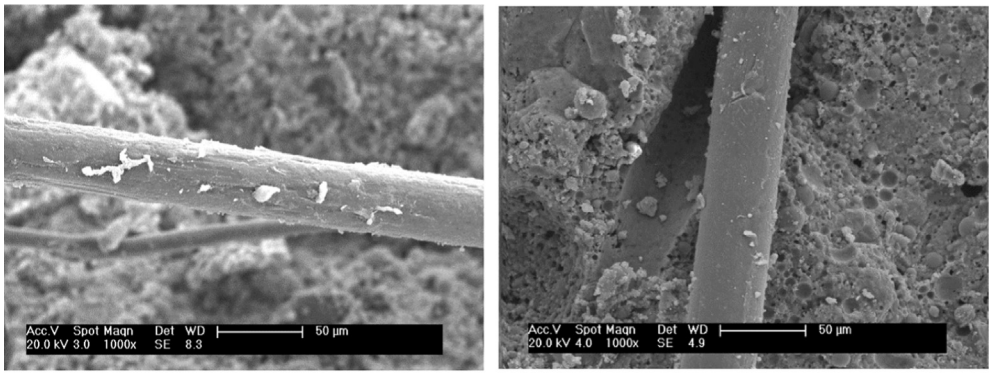

Fig. 8. The PVA fiber surface conditions after pulled out in EA-ECCs: (a) EA-ECC0; (b) EA-ECC25.

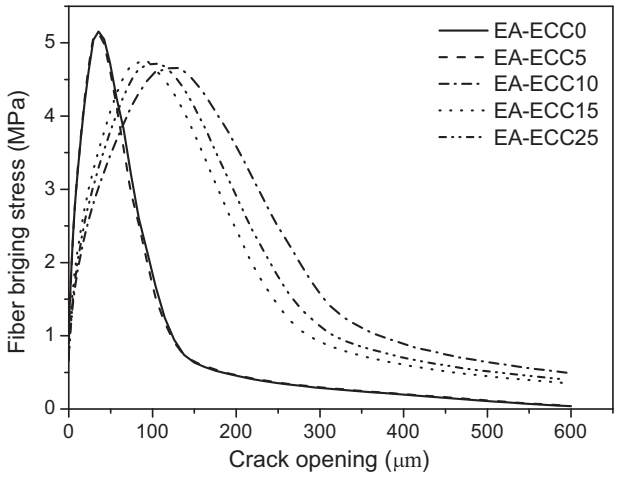

Fig. 9. Fiber bridging stress versus crack opening curves of EA-ECCs.

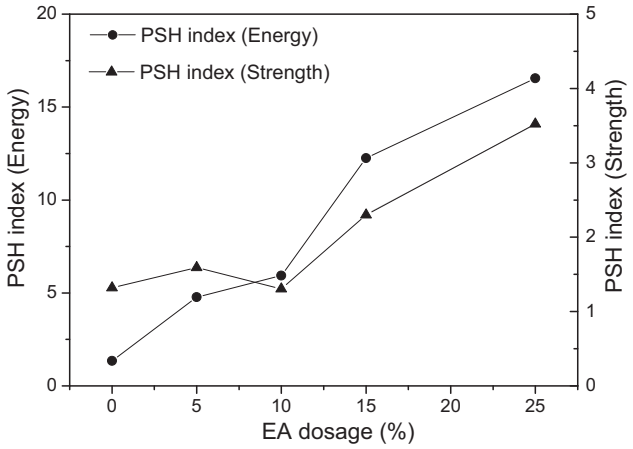

Fig. 11. PSH indexes of EA-ECCs versus EA dosage.

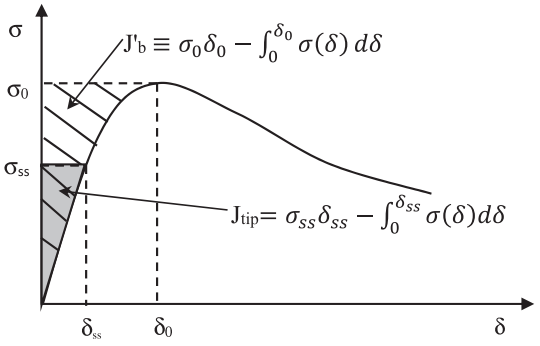

Fig. 10. Definition of crack tip toughness J_{tip} and complementary energy J_b' in typical curve of fiber bridging stress σ versus crack opening width δ.

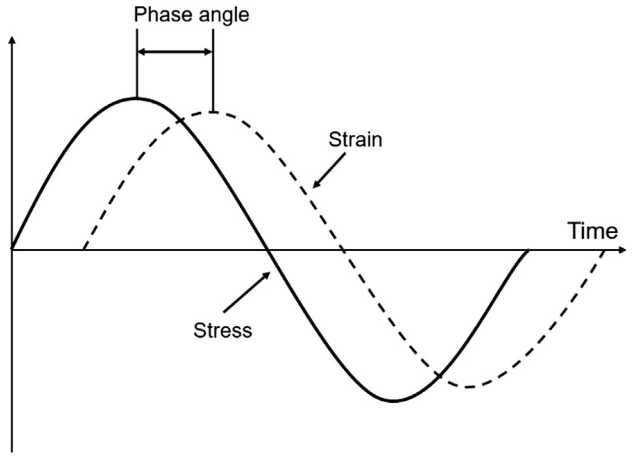

Fig. 12. The response of viscoelastic material when subjected to a sinusoidal load.

The loss factor (tan δ) defined as the ratio of energy dissipated as heat to the maximum energy stored in the material, characterizes the damping performance of the material, and can be expressed in Eq. (8) [22].

$$\tan\delta = \frac{E''}{E'} \tag{8}$$

The storage modulus of all EA-ECCs decreases gradually with increasing temperature, as shown in Fig. 13. Compared to emulsified asphalt, cementitious hydration products and sand are elastic solid, therefore, the viscoelasticity variation of EA-ECC is mainly determined by asphalt. At low temperature, the molecular chains of asphalt are frozen, only chain angle and chain length can be changed slightly under dynamic loading, which results in a higher storage modulus of EA-ECCs. With increasing temperature, the asphalt gradually translates to rubber or viscous fluid states, which increases the free volume in asphalt. In this case, the molecular chains of asphalt can be moved and elongated easily under

dynamic loading, which increases the flexibility and reduces the storage modulus of EA-ECCs. In the case of EA-ECC0, the storage modulus also exhibits a reduction trend with increasing temperature. The water in pores of EA-ECC is in ice state at low temperature, and gradually melted with increasing temperature, which results in the reduction of storage modulus [32].

The storage modulus of EA-ECCs decreases with increasing EA dosage at the same temperature, as shown in Fig. 13. The matrix of EA-ECC consists of cementitious (cement and fly ash) hydration products, silica sand and emulsified asphalt. When the ratio of asphalt to cement (EA/C) is low, cementitious hydration products constitute the continuous phase in matrix, while the asphalt serves as the disperse phase in matrix. In addition, cementitious hydration products have a higher stiffness than asphalt, which causes a large storage modulus of EA-ECC when EA/C is low. With increasing EA/C, the asphalt gradually translates from disperse phase to more continuous phase, which reduces the storage modulus of EA-ECC.

With increasing temperature, the loss modulus of EA-ECCs increase gradually until reaching a maximum between 25 and 40 °C and decreases subsequently as shown in Fig. 14. The loss modulus reflects the energy dissipation ability of a viscoelastic material under dynamic alternating loads, which relates to the work done by internal friction force of molecular chain. At low temperature, the molecular chain of asphalt has a large internal friction force, while the slippage of molecular chain is very small because it is in frozen state. Therefore, the work done by internal friction force of molecular chain is very small, that is why EA-ECCs have a small loss modulus at low temperature. With increasing temperature, the molecular chain can slip easily, which is beneficial for the work done by internal friction force. In addition, the water melting in pore also gradually dissipate energy. Thus, the loss modulus of EA-ECCs increase with temperature. However, with further temperature increase, the internal friction force of molecular chain reduces rapidly [24], which is adverse for dissipating energy, and decreases the loss modulus of EA-ECCs. Thus, when the temperature passes the critical value, reduction of internal friction force on work dominates that of slippage increase of molecular chain, leading to a reduction of loss modulus, as shown in Fig. 15.

As can be seen in Fig. 14, the loss modulus of EA-ECCs generally increase with higher ratio of EA to cement. High EA dosage means that there are more molecular chain participate in work done by internal friction force, which causes the large loss modulus of EA-ECC. On the other hand, the deformation of asphalt phase was obstructed by cementitious hydration products phase at low

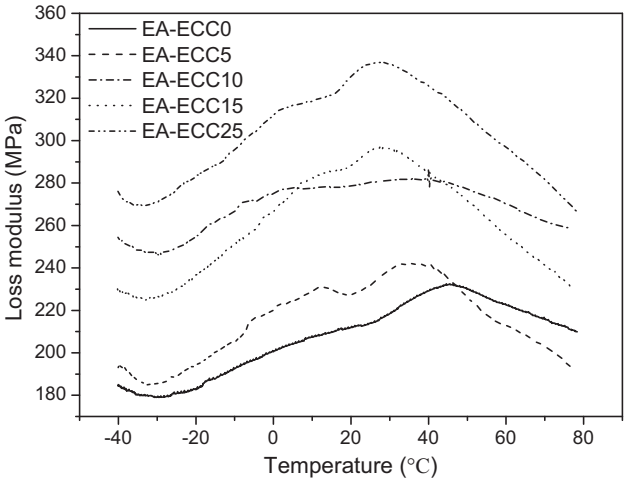

Fig. 14. Loss modulus of EA-ECCs with increasing temperature.

EA/C, which postpones the reduction of internal friction force with increasing temperature. Therefore, the maximum loss modulus occurs at a higher temperature for EA-ECC with lower EA/C. The result indicates that EA-ECCs with more emulsified asphalt (higher EA/C) can achieve the maximum energy dissipation ability at a lower temperature compare to those ECCs with lower EA/C.

Loss factor (tan δ) characterizes the phase angle between given stress and measured strain of one material under dynamical load, which reflects the damping ability of a viscoelastic material [33]. As can be seen in Fig. 16, the loss factors of EA-ECCs increase and subsequently stabilize or decrease with temperature. As cementitious hydration products can be regarded as elastic ingredient compared with asphalt, the phase angle of EA-ECC is mainly governed by emulsified asphalt. At low temperature, asphalt is in the glass state and can be seen as elastic solid, resulting in a small phase angle and loss factor. With increasing temperature, the viscoelasticity of the asphalt phase gradually enlarge the phase angle, which increases the energy dissipation and damping ability of EA-ECCs. With further temperature increase, however, the asphalt gradually translates to viscous fluid state. The cementitious hydration products carry all the external dynamic loads, which causes the phase angle of EA-ECCs descends and subsequently reduces the loss factor, as shown in Fig. 16.

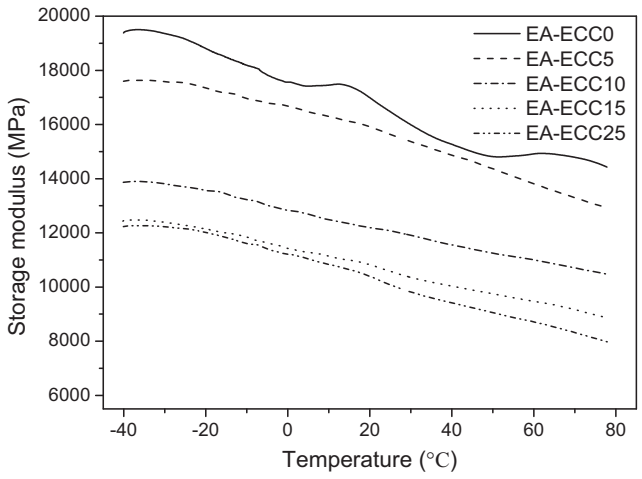

Fig. 13. Storage modulus of EA-ECCs with increasing temperature.

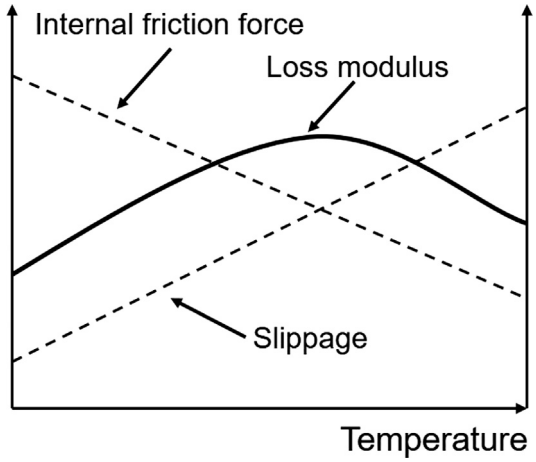

Fig. 15. Schematic view of trend of internal friction force, slippage of molecular chains and loss modulus.

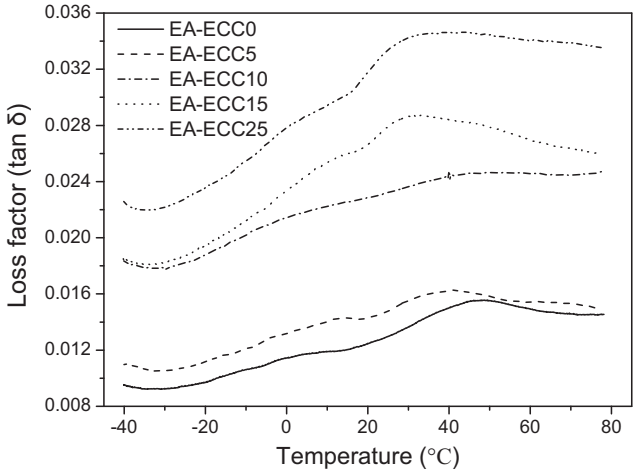

Fig. 16. Loss factor (tan δ) of EA-ECCs with increasing temperature.

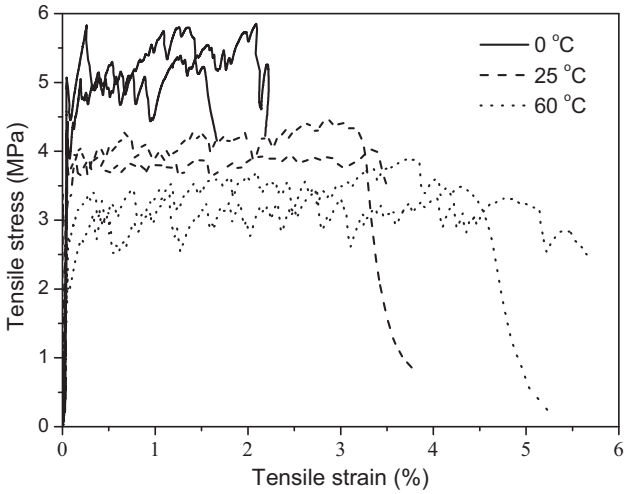

Fig. 18. Tensile stress-strain curves of EA-ECC10 under different test temperature.

As expected, the loss factors of EA-ECCs increase with EA dosage, as shown in Fig. 16. At low EA/C, the asphalt is disperse phase in composite, the damping property of EA-ECC is dominated by the continuous phase of cementitious hydration products. With increasing EA dosage, the viscoelastic of asphalt phase has a more and more significant impact on the damping property of EA-ECCs. Therefore, the EA-ECC with more emulsified asphalt exhibits a larger loss factor. The results indicates that incorporating emulsified asphalt can improve the damping ability and increase energy dissipation ability of ECC.

3.4. Temperature effect on mechanical properties of EA-ECC10

Due to significant thermal sensitivity of EA, mechanical properties of EA-ECCs under different test temperature need to be investigated. EA-ECC10 was selected for temperature sensitivity study of EA-ECC. The investigation results are shown in Figs. 17 and 18.

As can be seen in Fig. 17, compressive strength of EA-ECC10 reduces gradually with increasing test temperature. At low temperature of 0 °C, the compressive strength of EA-ECC10 is 54.5 MPa, which reduces to 40.8 MPa (reduces by 25%) at high test temperature of 60 °C. As mentioned previously, asphalt membrane in EA-ECC retards the linking of cementitious hydration products (C-S-H), which impedes the formation of a strong C-S-H network. However, EA in EA-ECC also has a hardening effect at low temperature. The frozen asphalt membrane may form a strong network together with C-S-H, which results in a higher compressive strength. Conversely, EA has a softening trend with increasing test temperature, which results in a weak network and further reduces the compressive strength of EA-ECC10. In addition, the pore-water and hydration products within cementitious materials normally freeze at temperature below 0 °C, which could be another reason for higher compressive strength of EA-ECC10 at low temperature.

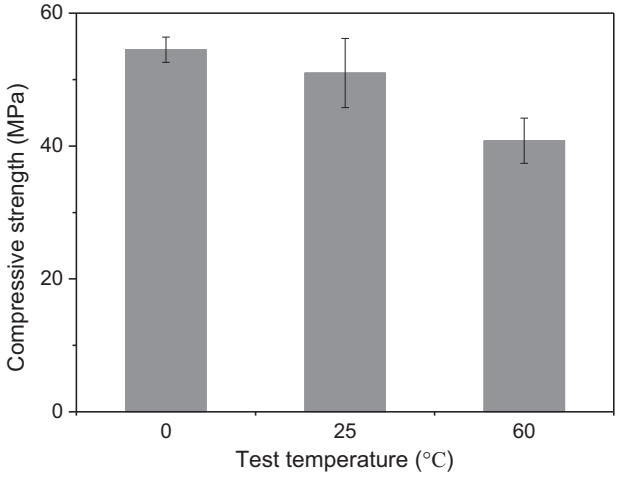

Fig. 17. Compressive strength of EA-ECC10 under different test temperature.

The influence of test temperature on tensile stress-strain behavior of EA-ECC10 is shown in Fig. 18. As can be seen, first cracking strength decreases with increasing test temperature, which is consistent with the trend in compressive strength. As mentioned before, EA has a softening trend with increasing test temperature. In addition, bond between asphalt membrane and particles (cementitious hydration products and silica sand) may decrease with test temperature. Therefore, initial flaw in EA-ECC10 matrix may be extended to a crack more easily under tensile load, which results in a lower fracture strength of matrix (consistent with first cracking strength). The tensile strength of EA-ECC10 also decrease with test temperature. It reduces by 36% when test temperature is increased form 0 °C to 60 °C. As discussed in Section 3.2, the fiber bridging capacity is closely related to interface frictional bond strength which is governed by ITZ properties. At low test temperature, the hardened EA leads to an increased hardness of ITZ, which may increase frictional bond strength, fiber bridging capacity and subsequently tensile strength of EA-ECC10.

Conversely, the tensile strain capacity of EA-ECC10 has an increasing trend with test temperature. As mentioned above, with higher frictional bond strength at low test temperature, the fibers may be impeded from being pulled out or even ruptured during slipping stage. At high test temperature, a reverse trend may be expected which is beneficial to multiple cracking behavior. These effects may reduce or increase the complementary energy J_b' of fiber bridging at low or high test temperature, respectively. Therefore, EA-ECC10 exhibits an improved tensile strain-hardening behavior, especially tensile strain capacity, with increasing test temperature.

4. Conclusions

In this paper, emulsified asphalt was employed to develop EA-ECC with high damping ability and excellent ductility simultaneously. The influence of EA dosage and test temperature on EA-ECC's mechanical properties, including compressive strength, ten-

sile stress-strain relation and dynamic mechanical properties, were investigated experimentally. The following conclusions can be drawn based on the research findings in this paper.

1) Incorporating EA in ECC effectively increases the loss modulus and loss factor of EA-ECCs which is beneficial to their energy dissipation and damping ability, while reduces the compressive strength with increase EA dosage.
2) The tensile deformation capacity of EA-ECCs was improved significantly with increase dosage of EA, while the tensile strength of EA-ECCs shows an obvious decrease trend with increasing EA/C. Nevertheless, tensile strength of EA-ECC can still reach 4.5 MPa when EA/C is 25%, which satisfies the requirement of most structural applications.
3) Temperature has a significant influence on EA-ECC's mechanical properties. With increasing temperature, the mechanical strengths of EA-ECC10, including compressive strength, first cracking strength and tensile strength, decrease noticeably, while the deformation capacity increases significantly.

The developed new materials can potentially be adopted as vibration absorbing layer between the roadbed and track slab of high speed railway and other similar applications where both high tensile ductility and energy dissipation capability are required.

Conflict of interest

The authors declare no conflict of interest.

References

[1] V.C. Li, From micromechanics to structural engineering - the design of cementitious composites for civil engineering application, J. Struct. Eng. Earthq. Eng. 10 (2) (1993) 37–48.
[2] V.C. Li, C.K.Y. Leung, Steady state and multiple cracking of short random fiber composites, J. Eng. Mech. 118 (11) (1992) 2246–2264.
[3] V.C. Li, H. Stang, H. Krenchel, Micromechanics of crack bridging in fibre-reinforced concrete, Mater. Struct. 26 (8) (1993) 486–494.
[4] V.C. Li, On engineered cementitious composites (ECC). A review of the material and its applications, J. Adv. Concr. Technol. 1 (3) (2003) 215–230.
[5] S.X. Wang, V.C. Li, Engineered Cementitious Composites with High-Volume Fly Ash, ACI Mater. J. 104 (3) (2007) 233–241.
[6] K. Yu, Y. Wang, J. Yu, S. Xu, A strain-hardening cementitious composites with the tensile capacity up to 8%, Constr. Build. Mater. 137 (2017) 410–419.
[7] V.C. Li, S.X. Wang, C. Wu, Tensile strain-hardening behavior of polyvinyl alcohol engineered cementitious composite (PVA-ECC), ACI Mater. J. 98 (6) (2001) 483–492.
[8] M. Kunieda, K. Rokugo, Recent progress on HPFRCC in Japan required performance and applications, J. Adv. Concr. Technol. 4 (1) (2006) 19–33.
[9] M.D. Lepech, V.C. Li, Application of ECC for bridge deck link slabs, Mater. Struct. 42 (9) (2009) 1185–1195.
[10] C. Esveld, Recent development in slab track, Eur. Railw. Rev. 2 (2003) 81–85.
[11] F. Wang, Z. Liu, T. Wang, S. Hu, A novel method to evaluate the setting process of cement and asphalt emulsion in CA mortar, Mater. Struct. 41 (4) (2008) 643–647.
[12] W. Qiang, Y. Peiyu, A. Ruhan, Y. Jinbo, K. Xiangming, Strength mechanism of cement-asphalt mortar, J. Mater. Civ. Eng. 23 (9) (2011) 1353–1359.
[13] S.Y. Zhu, Q. Fu, C.B. Cai, P.D. Spanos, Damage evolution and dynamic response of cement asphalt mortar layer of slab track under vehicle dynamic load, Sci. China Technol. Sci. 57 (10) (2014) 1883–1894.
[14] GB175-2007, Common Portland cement, 2007.
[15] GB1596-88, Fly ash Used in Cement and Concrete, 1988.
[16] Y.J. Xie, G.J. Zhen, C. Jiang, Z. Zeng, Z.C. Weng, Passenger Dedicated Line Railway Provisional Technical Conditions CRTS II Type of Slab Track Emulsified Asphalt Cement Mortar, China Railway Publish House, Beijing, 2008.
[17] M.D. Lepech, V.C. Li, Water permeability of engineered cementitious composites, Cem. Concr. Compos. 31 (10) (2009) 744–753.
[18] Japan Society of Civil Engineers, Recommendations for design and construction of high performance fiber reinforced cement composites with multiple fine cracks (HPFRCC), vol. 82, 2008.
[19] H. Ma, J.M. Cai, Z. Lin, S.Z. Qian, V.C. Li, $CaCO_3$ whisker modified engineered cementitious composite with local ingredients, Constr. Build. Mater. 151 (2017) 1–8.
[20] C. Redon, V.C. Li, C. Wu, H. Hoshiro, T. Saito, A. Ogawa, Measuring and modifying Interface properties of PVA fibers in ECC matrix, J. Mater. Civ. Eng. 13 (6) (2001) 399–406.
[21] American Society of Testing and Materials, "Standard test method for linear-elastic plane-strain fracture toughness KIc of metallic materials" 2013.
[22] Q. Yuan, L. Wentao, Y. Pan, D. Deng, Z. Liu, Characterization of cement asphalt mortar for slab track by dynamic mechanical thermoanalysis, J. Mater. Civ. Eng. 28 (3) (2016) 864–870.
[23] Z. Chen, E.-H. Yang, Y. Yang, Y. Yao, Latex-modified engineered cementitious composites (L-ECC), J. Adv. Concr. Technol. 12 (12) (2014) 510–519.
[24] Q. Fu, Y. Xie, G. Long, D. Niu, H. Song, Dynamic mechanical thermo-analysis of cement and asphalt mortar, Powder Technol. 313 (2017) 36–43.
[25] L.S. Tan, A.J. Mchugh, M.A. Gulgun, W.M. Kriven, Evolution of mechano-chemistry and microstructure of a calcium aluminate-polymer composite: part II. Mixing rate effects, J. Mater. Res. 11 (7) (1996) 1739–1747.
[26] S. Rodger, S. Brooks, W. Sinclair, High strength cement pastes, J. Mater. Res. 20 (1985) 2853–2860.
[27] E.H. Yang, Y.Z. Yang, V.C. Li, Use of high volumes of fly ash to improve ECC mechanical properties and material greenness, ACI Mater. J. 104 (6) (2007) 620–628.
[28] E.H. Yang, S.X. Wang, Y.Z. Yang, V.C. Li, Fiber-bridging constitutive law of engineered cementitious composites, J. Adv. Concr. Technol. 6 (1) (2008) 181–193.
[29] T. Kanda, V.C. Li, New micromechanics design theory for pseudostrain hardening cementitious composite, J. Eng. Mech. 125 (4) (1999) 373–381.
[30] V.C. Li, Engineered Cementitious Composites (ECC) – tailored composites through micromechanical modeling, Can. Soc. Civ. Eng. (1997) 1–38.
[31] L. Fang, Q. Yuan, Y. Pan, Y. Wang, K. Khayat, D. Deng, Temperature dependency of dynamic mechanical properties of cement asphalt paste by DMTA method, J. Wuhan Univ. Technol. Mater. Sci. Ed. 32 (6) (2017) 1379–1387.
[32] G. Foray-Thevenina, G. Vigiera, R. Vassoillea, G. Orangeb, Characterization of cement paste by dynamic mechanical thermo-analysis: part I: operative conditions, Mater. Charact. 56 (2) (2006) 129–137.
[33] X. Fu, D.D.L. Chung, Vibration damping admixtures for cement, Cem. Concr. Res. 26 (1) (1996) 69–75.